AIAA JOURNAL
Vol. 38, No. 3, March 2000

Instability of an Annular Liquid Sheet Surrounded by Swirling Airstreams

Y. Liao,* S. M. Jeng,† and M. A. Jog‡
University of Cincinnati, Cincinnati, Ohio 45221
and
M. A. Benjamin§
Parker Hannifin Corporation, Mentor, Ohio 44060

A theoretical model to predict the instability of an annular liquid sheet subjected to coaxial swirling airstreams is developed. The model incorporates essential features of a liquid sheet downstream of a prefilming airblast atomizer such as three-dimensional disturbances, inner and outer air swirl, finite film thickness, and finite surface curvature. Effects of flow conditions, fluid properties, and film geometry on the instability of the liquid sheet are investigated. It is observed that the relative axial velocity between the liquid and the gas phases enhances the interfacial aerodynamic instability by increasing the growth rate and the most unstable wave number. At low velocities, a combination of inner and outer airstreams is more effective in disintegrating the liquid sheet than only the inner or only the outer airstream. Also, the inner air is more effective than the outer air in promoting disintegration. Swirl not only increases the growth rate and the range of unstable wave numbers but also shifts the dominant mode from the axisymmetric mode to a helical mode. With the presence of air swirl, the most unstable wave number and the maximum growth rate are higher than their no-swirl counterparts. Inner air swirl increases the most unstable wave number more effectively than outer air swirl, and both airstreams swirling together leads to higher values of the maximum growth rate than do only inner or outer air swirl.

Nomenclature

A = vortex strength, m^2/s
c_j = coefficients in dispersion equation (23)
g = air/liquid density ratio
h = ratio of inner to outer radius, that is, R_a/R_b
I_n = nth-order modified Bessel function of first kind
K_n = nth-order modified Bessel function of second kind
k = axial wave number, 1/m
n = azimuthal wave number
P = mean pressure, N/m^2
p' = disturbance pressure, N/m^2
R_a = inner radius of the liquid sheet, m
R_b = outer radius of the liquid sheet, m
r = radial coordinate, m
t = time, s
U = mean axial velocity, m/s
u = disturbance axial velocity, m/s
V = mean radial velocity, m/s
v = disturbance radial velocity, m/s
W = mean tangential velocity, m/s
We = Weber number, $\rho U^2 R_b/\sigma$
w = disturbance tangential velocity, m/s
x = axial coordinate, m
η = displacement disturbance, m
θ = azimuthal angle, rad
λ = wavelength, m
ρ = fluid density, kg/m^3
Ω = angular velocity, 1/s
ω = temporal frequency, 1/s

Subscripts

i = inner gas
l = liquid phase
o = outer gas
s = based on swirling component

Introduction

MODERN combustion engines must meet increasingly stringent requirements regarding pollutant emissions, such as NO_x, in addition to improved combustion efficiency. The achievement of this goal depends largely on the performance of liquid fuel atomizer and rapid, uniform fuel–air mixing. The prefilming airblast atomizer has been considered as an advanced fuel injection concept and is widely used in gas turbine engines and oil-fired furnaces due to its advantages such as a low fuel pressure requirement, a large flow turndown ratio, and low pollutant emissions. Inside the atomizer, fuel is first forced into an annular passage to form a thin annular liquid sheet and is then exposed to high-speed swirling airstreams on both sides, as shown in Fig. 1. The strong shear action of swirling airstreams speeds up the disintegration process of the liquid sheet.[1] The breakup of the liquid sheet has direct effects on the resultant spray characteristics such as mean drop size and droplet size distribution and, thus, affects combustion efficiency and pollutant formation. Understanding the factors that influence the disintegration process will benefit not only atomizer design and improvement but also numerical simulation of spray combustion.[2]

It is well known that the disintegration of the liquid sheet is due to the growth of unstable waves at the interface between the gas and the liquid sheet. Various forces such as aerodynamic force, inertial force, surface tension, shear force, and centrifugal force involved in the disintegration process compete to dominate the instability of the liquid sheet. Extensive theoretical and experimental studies[3–8] have been conducted on the instability of planar liquid sheets. These two-dimensional instability models were extended later to the annular

Presented as Paper 98-3832 at the AIAA/ASME/SAE/ASEE 34th Joint Propulsion Conference, Cleveland, OH, 13–15 July 1998; received 22 January 1999; revision received 21 July 1999; accepted for publication 22 July 1999.

*Research Assistant Professor, Department of Aerospace Engineering and Engineering Mechanics.
†Associate Professor, Department of Aerospace Engineering and Engineering Mechanics. Member AIAA.
‡Associate Professor, Department of Mechanical, Industrial, and Nuclear Engineering.
§Technical Team Leader, Gas Turbine Fuel Systems Division. Member AIAA.

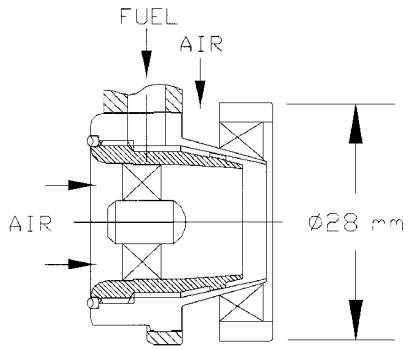

Fig. 1 Schematic of a prefilming airblast atomizer.

liquid sheet.[9–16] Effects of relative velocity between the liquid and gas phase, air-to-liquid density ratio, film thickness, and surface curvature on the instability of the annular liquid sheet were investigated. However, the airflow conditions in these studies[9–12,16] were in the low-speed regime (We_i or $We_o \leq 8$), and the swirl effect on the instability of the annular liquid sheet has not been considered. The effect of liquid swirl was examined in several recent studies,[13–15] and the linear stability analysis was combined with a breakup model to predict mean droplet sizes for the pressure-swirl atomizer. Agreement with experimental data was reasonable.[15]

Inside practical prefilming airblast atomizers, swirl is imparted to both the inner and outer air streams as well as to the liquid fuel. Experimental investigations[17,18] have revealed that the swirling airstreams promote the disintegration of the liquid sheet, apart from enhancing mixing and stabilizing flame. In Ref. 15 a theoretical model considering the liquid swirl was developed. However, a detailed theoretical analysis of the disintegration of the annular liquid sheet that includes the effects of air swirl is not yet available in the literature. The objective of the present paper is to develop an analytical model for the instability of the annular liquid sheet downstream of a prefilming airblast atomizer. This model predicts the most unstable wave number and the maximum growth rate that can be used to predict mean drop size and the liquid sheet breakup length. It incorporates essential features such as three-dimensional disturbances, inner and outer air swirl, finite film thickness, and finite surface curvature. Effects of flow conditions, fluid properties, and film geometry on the instability of the liquid sheet are investigated. A parametric study has been carried out to understand the instability of the liquid sheet under swirl and nonswirl airflow conditions.

Mathematical Formulation

The stability model considers an annular liquid sheet subjected to coaxial swirling airstreams, as shown in Fig. 2. Both the liquid and the gas phases are assumed to be inviscid and incompressible. Basic flow velocities for the liquid and the inner and the outer gas are assumed to be $(U_l, 0, 0)$, $(U_i, 0, \Omega r)$, and $(U_o, 0, A/r)$, respectively. The combination of the solid body rotation and free vortex profile is quite similar to the tangential velocity profile in practical gas turbine combustors.[19] To maintain an annular shape of the liquid sheet, a constraint must be imposed on the assumed mean airflows and is described by Eq. (1):

$$P_i - P_o = \sigma(1/R_a + 1/R_b) \tag{1}$$

The governing equations are written in vector form as

$$\nabla \cdot \boldsymbol{V} = 0 \tag{2}$$

$$\rho\left(\frac{\partial \boldsymbol{V}}{\partial t} + \boldsymbol{V} \cdot \nabla \boldsymbol{V}\right) = -\nabla P \tag{3}$$

where

$$\boldsymbol{V} = \begin{pmatrix} U \\ V \\ W \end{pmatrix}$$

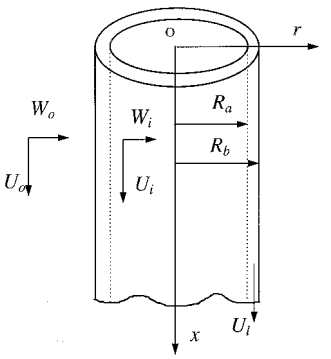

Fig. 2 Annular liquid sheet subjected to swirling airstreams.

To derive the linearized disturbance equations, velocity and pressure disturbances are superimposed on their mean counterparts as

$$\boldsymbol{V} = \bar{\boldsymbol{V}} + \boldsymbol{v}, \qquad p = P + p' \tag{4}$$

where

$$\boldsymbol{v} = \begin{pmatrix} u \\ v \\ w \end{pmatrix}$$

and the overbar represents the assumed mean flow quantities and the prime indicates disturbance. The velocity and pressure disturbances are assumed to have the forms of

$$(u, v, w, p') = [\hat{u}(r), \hat{v}(r), \hat{w}(r), \hat{p}(r)] \exp[i(kx + n\theta - \omega t)] \tag{5}$$

where the caret indicates disturbance amplitude, which is a function of r only. For temporal instability analysis, the wave number k and n are real, whereas the frequency ω is complex. The imaginary part of ω reflects the growth rate of a disturbance. The displacement disturbances at the inner and the outer interface are

$$\eta_j(x, \theta, t) = \hat{\eta}_j \exp[i(kx + n\theta - \omega t)], \qquad j = i, o \tag{6}$$

Note that no assumption has been made whether the two interfaces move in phase (antisymmetric mode) or out of phase (axisymmetric mode). The linearized disturbance equations for the liquid phase are written in vector form as follows:

$$\nabla \cdot \boldsymbol{v} = 0 \tag{7}$$

$$\rho_l\left(\frac{\partial \boldsymbol{v}}{\partial t} + U_l \frac{\partial \boldsymbol{v}}{\partial x}\right) = -\nabla p_l' \tag{8}$$

The linearized disturbance equations for the inner and outer air are written in component form as

$$\frac{\partial u}{\partial x} + \frac{v}{r} + \frac{\partial v}{\partial r} + \frac{1}{r}\frac{\partial w}{\partial \theta} = 0 \tag{9}$$

$$\frac{\partial u}{\partial t} + \frac{W_j}{r}\frac{\partial u}{\partial \theta} + U_j \frac{\partial u}{\partial x} = -\frac{1}{\rho_j}\frac{\partial p_j'}{\partial x} \tag{10}$$

$$\frac{\partial v}{\partial t} + U_j \frac{\partial v}{\partial x} + \frac{W_j}{r}\frac{\partial v}{\partial \theta} - \frac{2W_j w}{r} = -\frac{1}{\rho_j}\frac{\partial p_j'}{\partial r} \tag{11}$$

$$\frac{\partial w}{\partial t} + v\frac{\mathrm{d}W_j}{\mathrm{d}r} + \frac{W_j}{r}\frac{\partial w}{\partial \theta} + U_j \frac{\partial w}{\partial x} + \frac{W_j v}{r} = -\frac{1}{\rho_j}\frac{\partial p_j'}{r\partial \theta} \tag{12}$$

where $j = i, o$, $W_i = \Omega r$, and $W_o = A/r$.

Appropriate boundary conditions must be prescribed at the inner and outer surfaces of the liquid sheet to derive the dispersion

equation. The kinematic boundary conditions for the inner air, the outer air, and the liquid phase are described, respectively, by

$$v = \frac{\partial \eta_i}{\partial t} + \Omega\frac{\partial \eta_i}{\partial \theta} + U_i\frac{\partial \eta_i}{\partial x} \quad \text{at} \quad r = R_a \tag{13}$$

$$v = \frac{\partial \eta_o}{\partial t} + \frac{A}{r^2}\frac{\partial \eta_o}{\partial \theta} + U_o\frac{\partial \eta_o}{\partial x} \quad \text{at} \quad r = R_b \tag{14}$$

$$v = \frac{\partial \eta_i}{\partial t} + U_l\frac{\partial \eta_i}{\partial x} \quad \text{at} \quad r = R_a \tag{15}$$

$$v = \frac{\partial \eta_o}{\partial t} + U_l\frac{\partial \eta_o}{\partial x} \quad \text{at} \quad r = R_b \tag{16}$$

The dynamic boundary conditions at the inner and the outer interfaces are

$$p_l' - p_i' = \sigma\left(\frac{\eta_i}{R_a^2} + \frac{1}{R_a^2}\frac{\partial^2 \eta_i}{\partial \theta^2} + \frac{\partial^2 \eta_i}{\partial x^2}\right) + \rho_i \Omega^2 R_a \eta_i \quad \text{at} \quad r = R_a \tag{17}$$

$$p_l' - p_o' = -\sigma\left(\frac{\eta_o}{R_b^2} + \frac{1}{R_b^2}\frac{\partial^2 \eta_o}{\partial \theta^2} + \frac{\partial^2 \eta_o}{\partial x^2}\right) - \frac{\rho_o A^2 \eta_o}{R_b^3} \quad \text{at} \quad r = R_b \tag{18}$$

After extensive algebraic manipulations, the pressure disturbances in the inner air, the outer air, and the liquid sheet are expressed, respectively, by

$$p_i' = \frac{\rho_i\left[(-\omega + n\Omega + kU_i)^2 - 4\Omega^2\right](-\omega + n\Omega + kU_i)\hat{\eta}_i I_n(k_1 r)\exp[i(kx + n\theta - \omega t)]}{[(-\omega + n\Omega + kU_i)k_1 I_n'(k_1 R_a) + (2n\Omega/R_a)I_n(k_1 R_a)]} \tag{19}$$

$$p_o' = \frac{\rho_o}{k}\left(\omega - \frac{An}{R_b^2} - kU_o\right)\left(\omega - \frac{An}{r^2} - kU_o\right) \times \hat{\eta}_o \frac{K_n(kr)}{K_n'(kR_b)}\exp[i(kx + n\theta - \omega t)] \tag{20}$$

$$p_l' = \frac{\rho_l(-\omega + kU_l)^2}{k[I_n'(kR_a)K_n'(kR_b) - I_n'(kR_b)K_n'(kR_a)]} \times \{\hat{\eta}_i[K_n'(kR_b)I_n(kr) - I_n'(kR_b)K_n(kr)] + \hat{\eta}_o[I_n'(kR_a)K_n(kr) - K_n'(kR_a)I_n(kr)]\} \times \exp[i(kx + n\theta - \omega t)] \tag{21}$$

where $k_1 = k\sqrt{\{1 - [4\Omega^2/(-\omega + n\Omega + kU_i)^2]\}}$. The following dimensionless parameters are introduced to derive the nondimensional dispersion equation:

$$We_i = \frac{\rho_i U_i^2 R_b}{\sigma}, \quad We_o = \frac{\rho_o U_o^2 R_b}{\sigma}, \quad We_{\mathrm{so}} = \frac{\rho_o A^2}{\sigma R_b}$$

$$We_{\mathrm{si}} = \frac{\rho_i \Omega^2 R_b^3}{\sigma}, \quad We_l = \frac{\rho_l U_l^2 R_b}{\sigma}, \quad g_i = \frac{\rho_i}{\rho_l}$$

$$g_o = \frac{\rho_o}{\rho_l}, \quad h = \frac{R_a}{R_b}, \quad \bar{k} = kR_b, \quad \bar{\omega} = \frac{\omega R_b}{U_l} \tag{22}$$

The final nondimensional dispersion equation is fairly complicated and can be written as

$$c_7\bar{\omega}^4 + c_8\bar{\omega}^3 + c_9\bar{\omega}^2 + c_{10}\bar{\omega} - c_{11} - \frac{g_i\left\{-c_1\bar{\omega}^4 + c_{12}\bar{\omega}^3 + c_{13}\bar{\omega}^2 + c_{14}\bar{\omega} + c_{15}\right\}}{c_{16}I_n(h\bar{k}_1) + (-\bar{\omega} + c_4)\sqrt{1 - \left[c_5^{|}\ (-\bar{\omega} + c_4)^2\right]}I_n'(h\bar{k}_1)} \times (-\bar{\omega} + c_4)I_n(h\bar{k}_1) = 0 \tag{23}$$

where $\bar{k}_1 = \bar{k}\sqrt{\{1 - [c_5/(-\bar{\omega} + c_4)^2]\}}$. The coefficients $\{c_j\}$ in Eq. (23) depend on wave numbers $\bar{k}$ and n, flow conditions, fluid properties, and the geometric parameter and are given in the Appendix. The dispersion equation [i.e., Eq. (23)] does not have a closed-form solution. It was, thus, solved numerically by the secant method, which is an iterative method and requires two initial complex guess values. Without air swirl, the dispersion equation can be reduced to a fourth-order polynomial equation and can be readily solved analytically. When air swirl is present, guess values were taken from the solutions that correspond to nonswirling flow conditions. The solution was considered converged when the left-hand side of Eq. (23) was less than 10^{-8}. For each pair of $(\bar{k}, n)$ and given dimensionless parameters, the root with the maximum imaginary part that represents the growth rate of an unstable wave was obtained.

Results and Discussion

To predict accurately the disintegration of the annular liquid sheet emanating from practical prefilming airblast atomizers, the inner and outer airflows are assumed to have both axial and swirling velocity components in the model. Based on the nondimensional dispersion equation (23), a complete parametric study has been carried out to isolate the specific effect of flow conditions, fluid property, and nozzle geometry on the instability of the liquid sheet. The parameter space consists of the axial Weber numbers We_i, We_o, and We_l; the swirl Weber numbers We_{si} and We_{so}; the axial wave number $\bar{k}$; the azimuthal wave number n; the gas-to-liquid density ratios g_i and g_o; and the ratio of inner to outer radius h. The wave number (or frequency) with the maximum growth rate represents the most unstable wave and, hence, will dominate the liquid sheet breakup process. The speeds of surrounding air considered here are within the range of practical operating condition.[19]

Without Swirl

Figure 3 illustrates the effect of axial velocity on the dispersion diagram. It is seen from Fig. 3 that there exists a finite range of wave numbers with positive growth rate. There also exists a most unstable wave number corresponding to the maximum growth rate. This

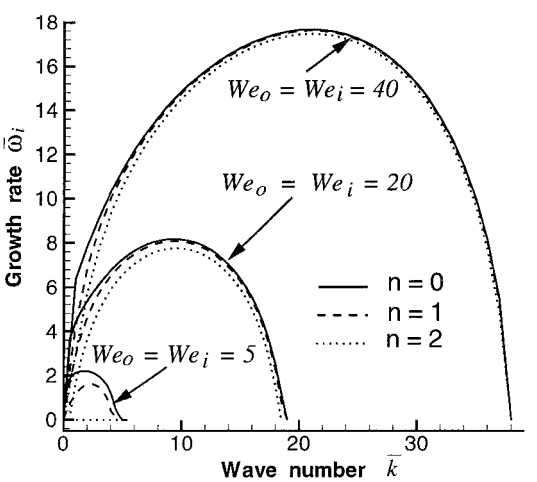

Fig. 3 Effect of axial velocity on dispersion diagram at $We_l = 37$, $g_i = g_o = 0.00129$, and $h = 0.93$.

behavior is explained as follows. The instability mechanism can be thought of as a frequency-selective amplifier. The mean flow is its energy supply, and its gain and frequency characteristics depend on flow parameters, fluid properties, and boundary conditions. When axial relative velocity is very low, the axisymmetric mode ($n=0$) dominates the competition of disturbance growth. As the axial velocity increases, both the maximum growth rate and the range of unstable wave numbers increases. Meanwhile, the most unstable wave number (or the dominant frequency) shifts to a higher value. This implies that the breakup length and mean drop size decrease with increasing relative velocity. This behavior is in agreement with available experimental results.[17,18] Furthermore, the importance of helical modes becomes comparable to that of the axisymmetric mode as the relative velocity increases.

The effectiveness of the combination of the axial flow of the inner and outer air in promoting aerodynamic instability of the liquid sheet is shown in Fig. 4a. At small Weber numbers (low velocity), the disturbance grows faster with inner and outer air moving than with

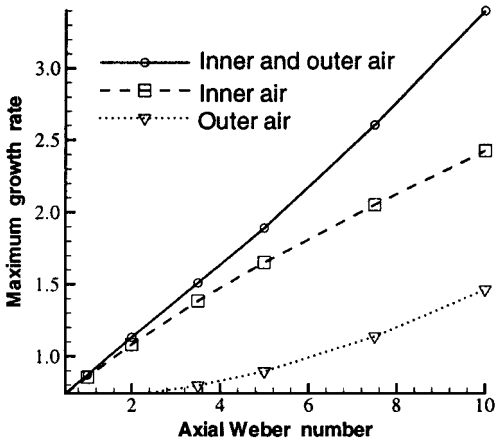

Fig. 4a Maximum growth rate vs axial Weber number at low velocity.

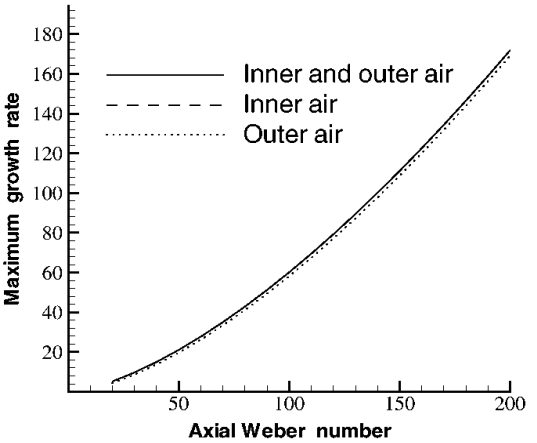

Fig. 5a Maximum growth rate vs axial Weber number at high velocity.

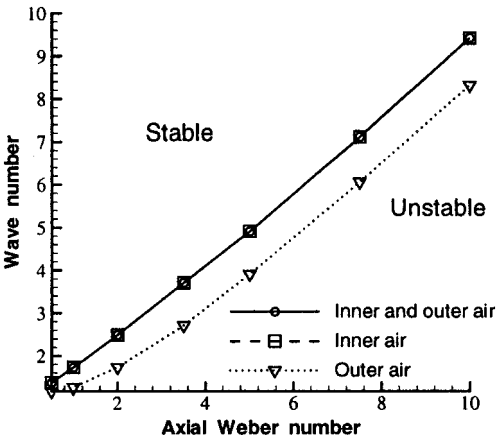

Fig. 4b Curve of neutral stability at low velocity.

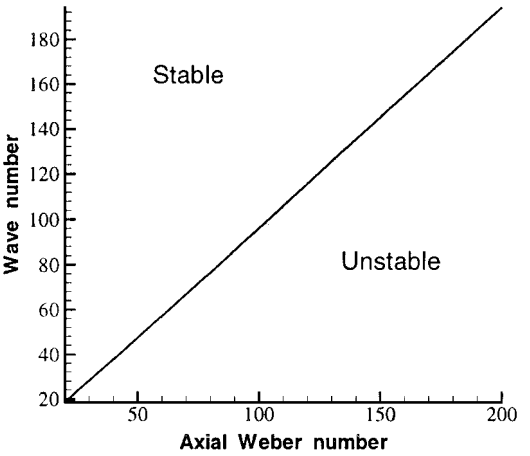

Fig. 5b Curve of neutral stability at high velocity.

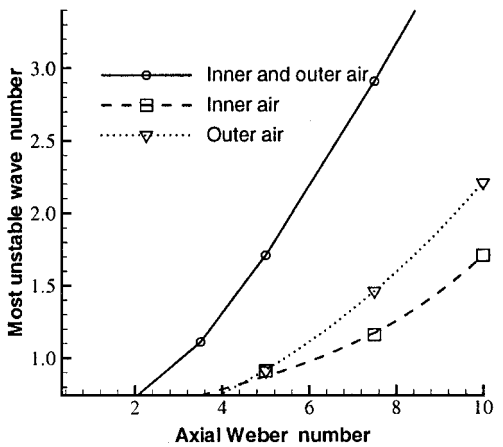

Fig. 4c Most unstable wave number vs axial Weber number at low velocity.

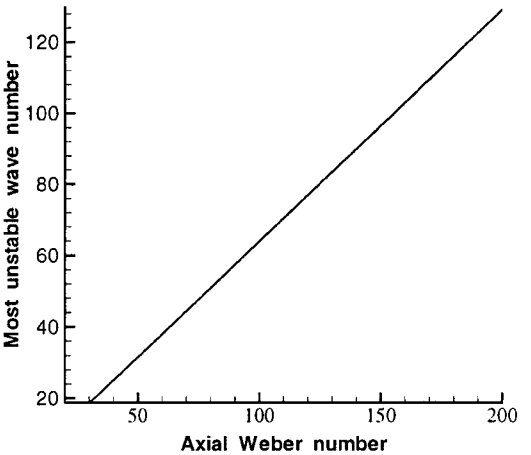

Fig. 5c Most unstable wave number vs axial Weber number at high velocity.

only inner or only outer air flow. This is because, with the presence of both inner and outer airstreams, the disturbance extracts energy from both the mean inner and outer flow. However, the range of unstable wave numbers and the most unstable wave number are the same as that associated with only inner air moving. By examining Fig. 4, we note that the inner air is more effective in enhancing aerodynamic instability than the outer air. The flow of the inner air leads to larger growth rates (Fig. 4a) and a wider range of unstable wave numbers (Fig. 4b). However, the flow has a smaller value of the most unstable wave number than its outer counterpart (Fig. 4c) when the axial Weber number is greater than 5.0. This behavior has been observed in previous experiments.[11] At large Weber numbers, as demonstrated by Fig. 5, the effectiveness of the inner and the outer air flow in making the liquid sheet unstable is almost the same as that with only the inner or the outer air. Moreover, the curve of neutral stability becomes a straight line and the relationship between axial Weber number and the most unstable wave number becomes linear. This is likely because of the dominant influence of the relative velocity at high speeds (Weber number).

The influence of the gas-to-liquid density ratio on the instability of annular liquid sheet is twofold as illustrated in Fig. 6. As can be clearly seen in Fig. 6a, the maximum growth rate decreases monotonically with density ratio. However, variation of the most unstable wave number with the density ratio displays two opposite trends. In the low-velocity regime, an increase in density ratio leads to a slight increase in the most unstable wave number. Because an increase in the gas density increases the aerodynamic interaction between liquid and gas phase, it enhances aerodynamic instability

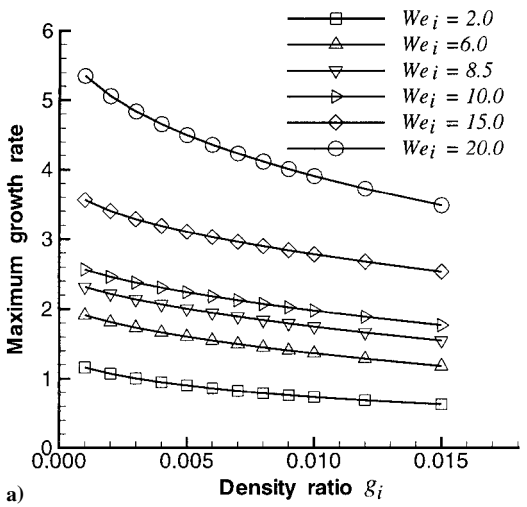

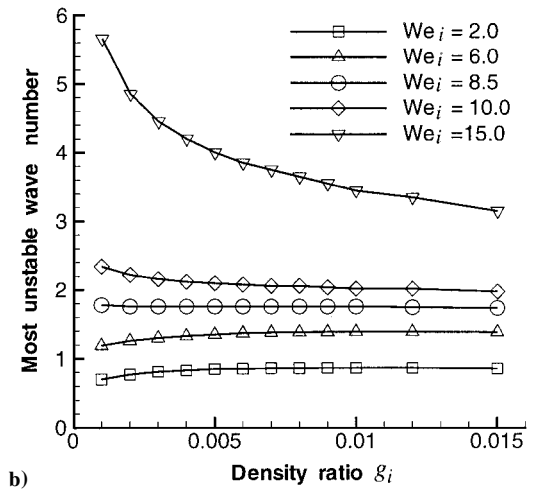

Fig. 6 Effect of density ratio on maximum growth rate and most unstable wave number at $We_o = 0$, $g_o = 0.00129$, and $h = 0.90$.

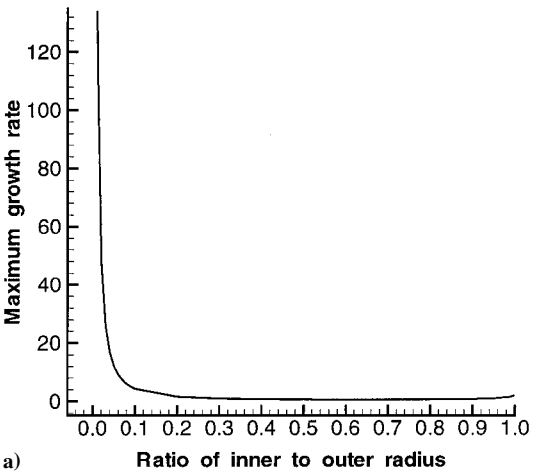

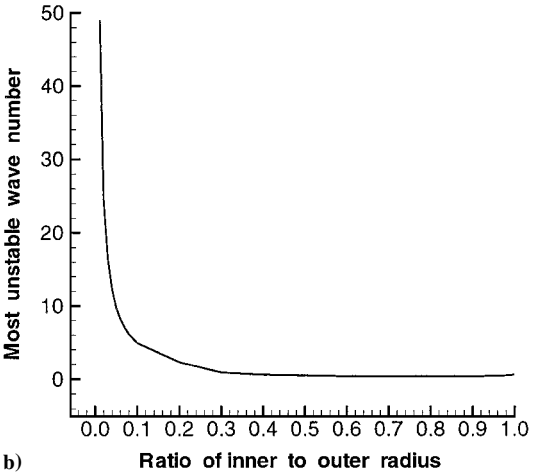

Fig. 7 Effect of surface curvature on maximum growth rate and most unstable wave number at $We_i = We_o = 0$, $We_l = 37$, and $g_i = g_o = 0.00129$.

of the liquid sheet. This implies that, at low velocity, the higher the ambient pressure, the smaller the drops produced. This conclusion has also been reported in a previous experimental study of the effect of ambient density on the drop size formed.[20] In contrast, in the high-velocity regime ($We_i \geq 8$), the most unstable wave number decreases with the density ratio. However, the resulting droplet size depends on both the most unstable wave number and the film thickness at the breakup location, which are determined by the maximum growth rate. Therefore, the net effect of the density ratio on the drop size becomes fairly complex. Such a complex behavior has also been observed in a previous study of aerodynamic breakup of liquid sheets.[21]

When the liquid sheet and the ambient air are both moving very slowly, surface curvature has a remarkable effect on the growth rates of unstable waves as shown in Fig. 7. For fixed film thickness, the maximum growth rate and the most unstable wave number first decrease sharply and then increase slightly with the radius of the inner surface. The transition takes place where h has a value of about 0.75. This is due to the competition between aerodynamic force and surface tension in influencing the growth of unstable waves. When the inner radius is very small, that is, when h is very small, the surface tension is responsible for the instability of the annular liquid sheet. As the inner radius increases, surface tension force decreases and, thus, leads to a lower growth rate and smaller most unstable wave number. However, as the inner radius increases further, the aerodynamic force becomes more important than the surface tension force and causes an increase in the growth rate and the most unstable wave number. This behavior is consistent with results reported in a previous study.[9]

Effect of Air Swirl

As illustrated in Fig. 8, features of the instability of the annular liquid sheet change significantly when swirl is added to the airstreams. Without swirl, as shown in Fig. 8a, the axisymmetric mode has the highest growth rate and, thus, dominates the competition in the disintegration process. However, when swirl is added to the inner airstream, the maximum growth rate and the most unstable wave number are increased, as shown in Fig. 8b. Helical modes are enhanced within the high-wave-number region. This indicates that short waves absorb more energy from the swirling inner airflow than long waves. The swirl needed to switch the dominant mode from the axisymmetric mode to a helical mode is very weak due to the inviscid assumption. Figure 8c is the dispersion diagram when swirl is added to the outer airstream. The swirl promotes helical modes within the whole unstable region instead of only the high-wave-number region as with the inner air swirl case. However, swirl inhibits the growth of the axisymmetric mode. Meanwhile, the increase in the maximum growth rate and the most unstable wave number of helical modes caused by the outer air swirl is smaller than the increase caused by its inner swirl counterpart. This implies that inner air swirl is more effective than outer air swirl in increasing the most unstable wave number and the maximum growth rate. As a result, it leads to smaller droplets and shorter breakup length. When swirl is added to both airstreams, as shown in Fig. 8d, the maximum growth rate is increased more significantly than that of only the single swirl cases. This is because unstable waves extract more energy from both swirling airstreams. Additionally, we found that, when the value of swirl Weber number is less than 10, the most unstable wave number is almost identical to that of only the inner swirl case but larger than its no-swirl counterpart. This demonstrates that swirl has a destabilizing effect on the annular liquid sheet. It leads to shorter breakup length and smaller droplet sizes than the situation where swirl is absent.

The growth rates of the first three modes for the cases of no swirl, only inner air swirl, only outer air swirl, and both air swirls are compared in Fig. 9. It is evident that the enhancement of helical modes due to swirl is far more significant than that of the axisymmetric mode. For helical modes, the combination of inner and outer air swirl leads to higher growth rates than that with only single air swirl. However, for the axisymmetric mode, outer air swirl causes a lower growth rate than its no-swirl counterpart.

Variations of the maximum growth rate and the most unstable wave number for the second helical mode ($n = 2$) are plotted against the swirl Weber number in Fig. 10. The swirl Weber numbers are within the range of practical operating conditions and are considered to have the same values as the axial Weber numbers. This is similar to the practical flow conditions downstream of airblast atomizer. The destabilizing effect of air swirl can be clearly seen from Fig. 10. With the presence of air swirl, the maximum growth rate and the most unstable wave number are increased. This trend has also been observed in a previous experiment.[17] As the swirl strength increases, the maximum growth rate and the most unstable wave number increase monotonically. The maximum growth rate has the highest value when swirl is added to both inner and outer air. Inner air swirl leads to higher growth rates than that caused by outer air swirl, as discussed before. Meanwhile, inner air swirl has the highest value

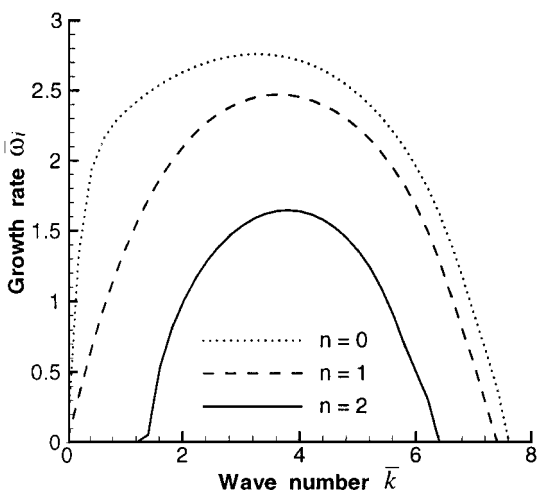

a) Without swirl

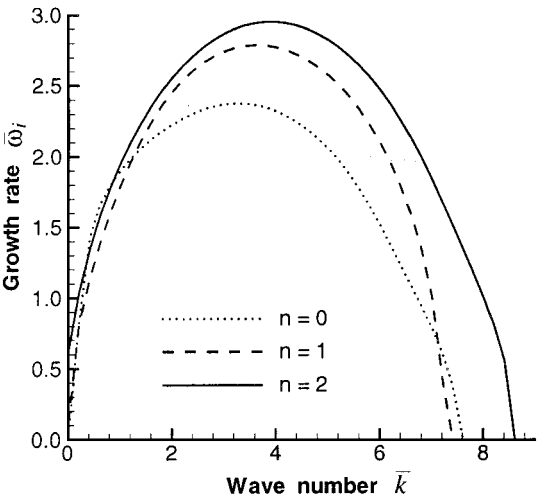

c) With only outer air swirl ($We_{so} = 8$)

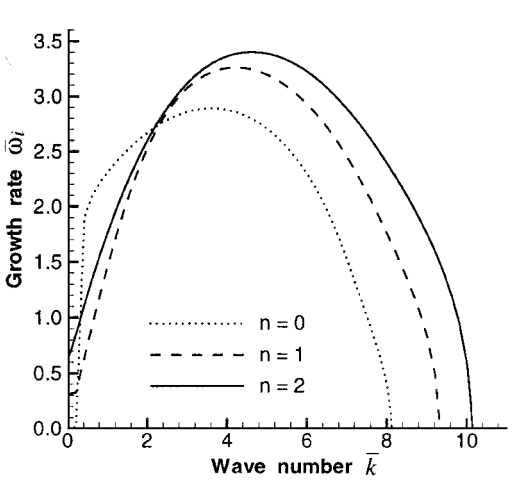

b) With only inner air swirl ($We_{si} = 8$)

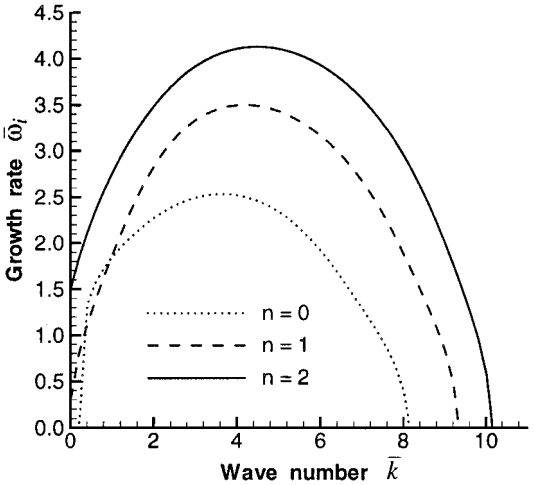

d) With both inner and outer swirl ($We_{si} = We_{so} = 8$)

Fig. 8 Growth rate vs wave number at $We_i = We_o = 8$, $We_l = 37$, $g_i = g_o = 0.00129$, and $h = 0.90$.

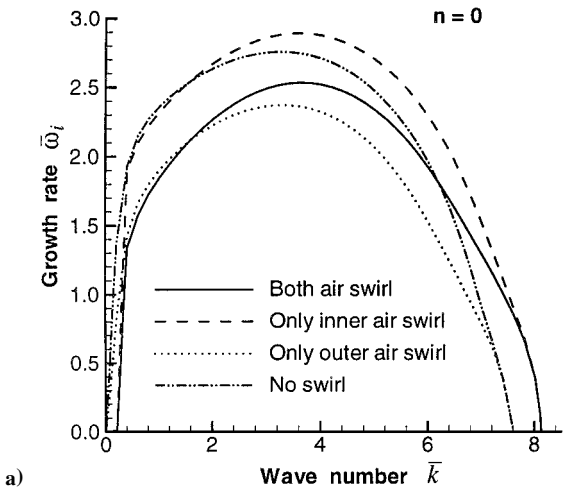

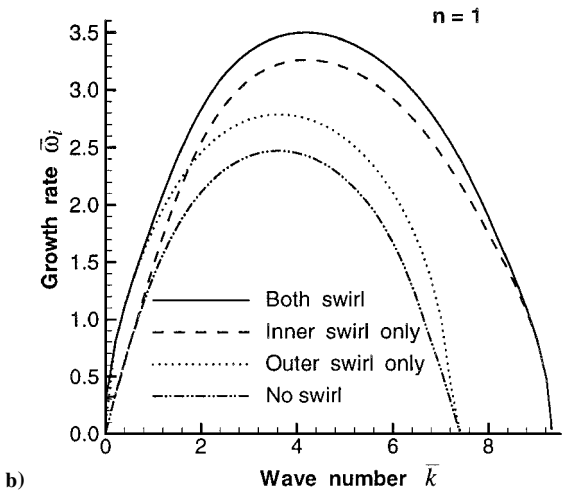

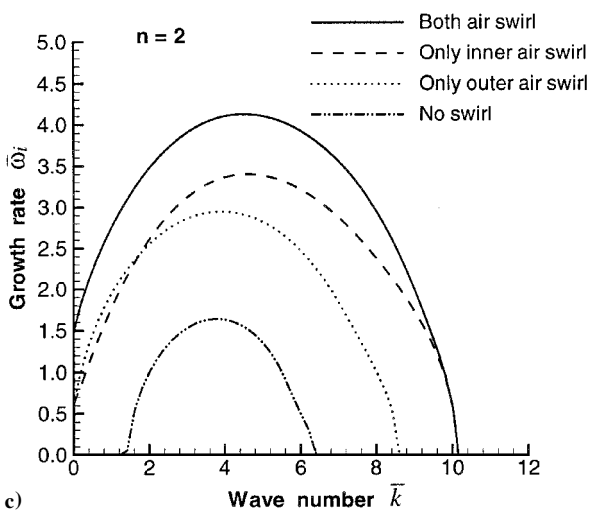

Fig. 9 Effect of air swirl on a) axisymmetric mode, b) first helical mode, and c) second helical mode at $We_i = We_o = 8$, $We_l = 37$, $g_i = g_o = 0.00129$, and $h = 0.90$.

of the most unstable wave number. This implies that, when swirl gets very strong, the combination of inner and outer swirl is less effective than only the inner air swirl in forming smaller droplets, although it speeds up the breakup process of the liquid sheet. In summary, inner air swirl is more effective in increasing the maximum growth rate and the most unstable wave number than outer air swirl. Therefore, it is conducive to improvement in the performance of airblast atomizers.

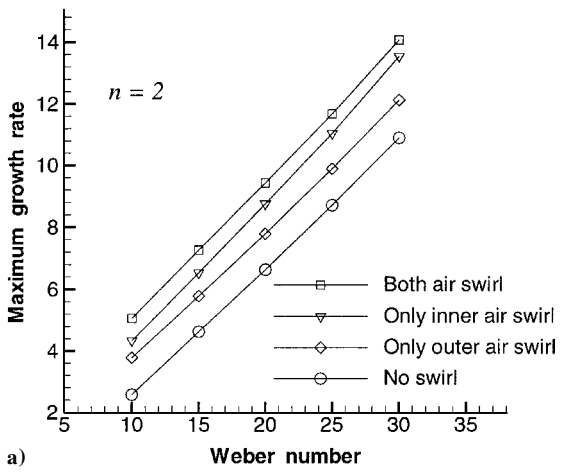

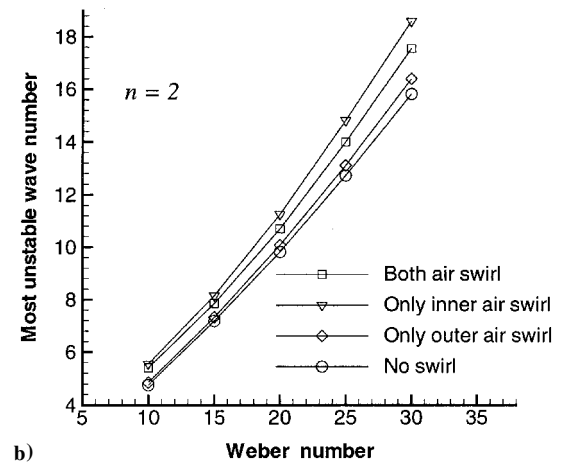

Fig. 10 Effect of air swirl on maximum growth rate and most unstable wave number at $We_l = 37$, $g_i = g_o = 0.00129$, and $h = 0.90$.

Conclusions

A theoretical model to predict the instability of an annular liquid sheet subjected to coaxial swirling airstreams is developed. The model incorporates essential features of the liquid sheet downstream of a prefilming airblast atomizer such as three-dimensional disturbances, inner and outer air swirl, finite film thickness, and finite surface curvature. Effects of flow conditions, fluid properties, and film geometry on the instability of liquid sheets are investigated. It is observed that the relative axial velocity between the liquid and the gas phases enhances the interfacial instability by increasing the growth rate and the most unstable wave number. At low velocities, the combination of inner and outer airstreams is more effective in disintegrating the liquid sheet than only the inner or only the outer airstream. Also, the inner air is more effective than the outer air in promoting disintegration. The effect of density ratio on the instability of the liquid sheet is twofold. In the low-velocity regime, an increase in the density ratio leads to a slight increase in the most unstable wave number. However, in the high-velocity regime ($We_i \geq 8$), the most unstable wave number decreases with the density ratio. When both the liquid sheet and the ambient air are moving very slowly, for fixed film thickness, both the maximum growth rate and the most unstable wave number first decrease sharply and then increase slightly with the radius of the inner surface. The transition takes place where h has a value of about 0.75. Enhancement of helical modes due to swirl is far more significant than that of the axisymmetric mode. Air swirl not only increases the maximum growth rate and the most unstable wave number but also shifts the dominant mode from the axisymmetric mode to a helical mode. With the presence of inner air swirl, the most unstable wave number and the maximum growth rate are higher than no-swirl and outer air swirl cases. The maximum growth rate has the highest value when swirl is added to both the inner and the outer

air. However, inner air swirl leads to the highest values of the most unstable wave number. Outer air swirl inhibits the growth of the axisymmetric mode but promotes helical modes.

Appendix: List of Coefficients

Coefficients c_1–c_{16} in dispersion equation (23) are as follows:

$$c_1 = -B_n + g_o G_n$$

$$c_2 = -2\bar{k}B_n + 2g_o\left(n\sqrt{\frac{We_{so}}{g_o We_l}} + \bar{k}\sqrt{\frac{We_o}{g_o We_l}}\right)G_n$$

$$c_3 = \frac{\bar{k}}{We_l}(1 - n^2 - \bar{k}^2) + \bar{k}\frac{We_{so}}{We_l} - \left(n\sqrt{\frac{We_{so}}{We_l}} + \bar{k}\sqrt{\frac{We_o}{We_l}}\right)^2 G_n + \bar{k}^2 B_n$$

$$c_4 = \left(n\sqrt{\frac{We_{si}}{We_l g_i}} + \bar{k}\sqrt{\frac{We_i}{We_l g_i}}\right), \qquad c_5 = \frac{4We_{si}}{We_l g_i}$$

$$c_6 = \frac{\bar{k}}{We_l h^2}(1 - n^2 - \bar{k}^2h^2) + \bar{k}h\frac{We_{si}}{We_l}, \qquad c_7 = c_1C_n - Q_nS_n$$

$$c_8 = -c_2C_n - 2c_1C_n\bar{k} + 4Q_nS_n\bar{k}$$

$$c_9 = -c_3C_n + 2c_2C_n\bar{k} + c_1C_n\bar{k}^2 - 6Q_nS_n\bar{k}^2 + c_1c_6$$

$$c_{10} = 2c_3C_n\bar{k} - c_2C_n\bar{k}^2 + 4Q_nS_n\bar{k}^3 - c_2c_6$$

$$c_{11} = c_3C_n\bar{k}^2 + Q_nS_n\bar{k}^4 + c_3c_6, \qquad c_{12} = c_2 + 2c_1c_4$$

$$c_{13} = c_3 - 2c_2c_4 - c_1c_4^2 + c_1c_5, \qquad c_{14} = -2c_3c_4 + c_2c_4^2 - c_2c_5$$

$$c_{15} = c_3c_4^2 - c_3c_5, \qquad c_{16} = \frac{2n}{h\bar{k}}\sqrt{\frac{We_{si}}{g_i We_l}}$$

where

$$G_n = \frac{K_n(\bar{k})}{K_n'(\bar{k})}, \qquad B_n = \frac{I_n'(\bar{k}h)K_n(\bar{k}) - K_n'(\bar{k}h)I_n(\bar{k})}{I_n'(\bar{k}h)K_n'(\bar{k}) - K_n'(\bar{k}h)I_n'(\bar{k})}$$

$$C_n = \frac{I_n'(\bar{k})K_n(\bar{k}h) - K_n'(\bar{k})I_n(\bar{k}h)}{I_n'(\bar{k}h)K_n'(\bar{k}) - K_n'(\bar{k}h)I_n'(\bar{k})}$$

$$S_n = \frac{I_n'(\bar{k})K_n(\bar{k}) - K_n'(\bar{k})I_n(\bar{k})}{I_n'(\bar{k}h)K_n'(\bar{k}) - K_n'(\bar{k}h)I_n'(\bar{k})}$$

$$Q_n = \frac{I_n'(\bar{k}h)K_n(\bar{k}h) - K_n'(\bar{k}h)I_n(\bar{k}h)}{I_n'(\bar{k}h)K_n'(\bar{k}) - K_n'(\bar{k}h)I_n'(\bar{k})}$$

Acknowledgments

This work was sponsored by NASA John H. Glenn Research Center at Lewis Field under Grant NAG3-1987 and by Parker Hannifin Corporation.

References

[1] Lefebvre, A. H., *Atomization and Sprays*, Hemisphere, New York, 1989, pp. 142–144.

[2] Rizk, N. K., Chin, J. S., and Razdan, M. K., "Modeling of Gas Turbine Fuel Nozzle Spray," *Journal of Engineering for Gas Turbines and Power*, Vol. 119, No. 1, 1997, pp. 34–44.

[3] Squire, H. B., "Investigation of the Instability of a Moving liquid film," *British Journal of Applied Physics*, Vol. 4, June 1953, pp. 167–169.

[4] Hagerty, W. W., and Shea, J. F., "A Study of the Stability of Plane Fluid Sheets," *Journal of Applied Mechanics*, Vol. 22, No. 4, 1955, pp. 509–514.

[5] Fraser, R. P., Eisenklam, P., Dombrowski, N., and Hasson, D., "Drop Formation from Rapidly Moving Liquid Sheets," *AIChE Journal*, Vol. 8, No. 5, 1962, pp. 672–680.

[6] Dombrowski, N., and Johns, W. R., "The Aerodynamic Instability and Disintegration of Viscous Liquid Sheets," *Chemical Engineering Science*, Vol. 18, No. 3, 1963, pp. 203–214.

[7] Clark, C. J., and Dombrowski, N., "Aerodynamic Instability and Disintegration of Inviscid Liquid Sheets," *Proceedings of the Royal Society of London, Series A: Mathematical and Physical Sciences*, Vol. 329, No. 1579, 1972, pp. 467–478.

[8] Li, X., and Tankin, R. S., "On the Temporal Instability of a Two-Dimensional Viscous Liquid Sheet," *Journal of Fluid Mechanics*, Vol. 226, May 1991, pp. 425–443.

[9] Crapper, G. D., Dombrowski, N., and Pyott, G. A. D., "Kevin–Helmholtz Wave Growth on Cylindrical Sheets," *Journal of Fluid Mechanics*, Vol. 68, April 1975, pp. 497–502.

[10] Meyer, J., and Weihs, D., "Capillary Instability of an Annular Liquid Jet," *Journal of Fluid Mechanics*, Vol. 179, June 1987, pp. 531–545.

[11] Lee, J. G., and Chen, L.-D., "Linear Stability Analysis of Gas-Liquid Interface," *AIAA Journal*, Vol. 29, No. 10, 1991, pp. 1589–1595.

[12] Shen, J., and Li, X., "Instability of an Annular Viscous Liquid Jet," *Acta Mechanica*, Vol. 114, 1996, pp. 167–183.

[13] Dumouchel, C., Ledoux, M., Bloor, M. I. G., Dombrowski, N., and Ingham, D. B., "The Design of Pressure Swirl Atomizers," *23th Symposium (International) on Combustion*, Combustion Inst., Pittsburgh, PA, 1990, pp. 1461–1467.

[14] Panchagnula, M. V., Sojka, P. E., and Santangelo, P. J., "On the Three-Dimensional Instability of a Swirling, Annular, Inviscid Liquid Sheet Subject to Unequal Gas Velocities," *Physics of Fluids*, Vol. 8, No. 12, 1996, pp. 3000–3312.

[15] Liao, Y., Sakman, A. T., Jeng, S. M., Jog, M. A., and Benjamin, M. A., "A Comprehensive Model to Predict Simplex Atomizer Performance," *Journal of Engineering for Gas Turbines and Power*, Vol. 121, No. 2, 1999, pp. 285–294.

[16] Shen, J., and Li, X., "Breakup of Annular Liquid Jets in Two Gas Streams," *Journal of Propulsion and Power*, Vol. 12, No. 4, 1996, pp. 752–759.

[17] Lavergne, G., Trichet, P., Hebrard, P., and Biscos, Y., "Liquid Sheet Disintegration and Atomization Process on a Simplified Airblast Atomizer," *Journal of Engineering for Gas Turbines and Power*, Vol. 115, No. 3, 1993, pp. 461–466.

[18] Carvalho, I. S., and Heitor, M. V., "The Break-Up of a Annular Liquid Sheet Downstream of an Airblast Prefilming Atomizer," *10th Symposium on Turbulent Shear Flows, Proceedings*, Vol. 3, Pennsylvania State Univ., University Park, PA, 1995, pp. 3-97–3-102.

[19] Rizk, N. K., and Mongia, H. C., "Model for Airblast Atomization," *Journal of Propulsion and Power*, Vol. 7, No. 3, 1991, pp. 305–311.

[20] Dombrowski, N., and Hooper, P. C., "The Effect of Ambient Density on Drop Formation in Sprays," *Chemical Engineering Science*, Vol. 17, April 1962, pp. 291–305.

[21] Ingebo, R. D., "Atomization of Liquid Sheets in High Pressure Airflow," NASA TM-83731, 1984.

J. P. Gore
Associate Editor